IECON 2021 - 47th Annual Conference of the IEEE Industrial Electronics Society | 978-1-6654-3554-3 /21/$31.00 ©2021 CRWN | DOI: 10.1109/IECON48115.2021.9589354

Pack-Level Electrochemical Impedance Spectroscopy in EV Batteries Enabled by a DC Fast Charger

Z. Gong[1], S. A. Assadi[1], S. Sarofim[1], M. Tessy[1], D. Lamont[1], A. Nowicki[1], J. Piruzza[1], K. Fatih[2], Y. Yoo[2], and O. Trescases[1]

[1]The Edward S. Rogers Sr. Department of Electrical and Computer Engineering, University of Toronto,
[2]Energy, Mining, and Environment Research Centre, National Research Council Canada,
Email: zhe.gong@mail.utoronto.ca

***Abstract*— In order to reliably operate Lithium-ion battery systems at their maximum power capability, it is advantageous to track the battery electrical impedance. Direct-Current Fast Charging (DCFC) stations provide a low-cost opportunity to introduce in-situ impedance measurements through the shared use of new hardware across many users. The feasibility of DCFC-based EV battery pack impedance measurement is explored in this work. To the authors' knowledge, this is the first published measurement and analysis of impedance data from a commercial EV dc charging plug. A custom 50 kW CHAdeMO-interface DCFC is implemented, featuring electrochemical impedance spectroscopy with 5 A perturbation current at 400V, up to 3.1 kHz. The high-voltage system impedance is measured for a prototype EV featuring a custom 27kWh battery pack, and a 2015 Nissan Leaf EV through the CHAdeMO port. It is found that while the vehicle-level impedance is significantly affected by the DCFC charging cable and internal vehicle components, battery impedance variation due to temperature can still be detected. This work motivates the future development of charger-side battery diagnostics, including 1) large-scale vehicle fleet battery health monitoring, 2) data collection for improved battery degradation modeling, and 3) direct information exchange with EVs for battery performance optimisation.**

I. Introduction

In 2020, 2 million electric vehicles and 50,000 Level-2 or DC-Fast Charging (DCFC) stations were in operation in North America [1], [2]. The continued growth of EV deployment requires efficient utilisation of the charging station infrastructure, which reduces the stations required per vehicle. In order to meet this objective, EV Battery Management Systems (BMS) must increase the usable capacity, power, and lifetime of the installed battery cells, and minimise DCFC power curtailment due to battery voltage/temperature limitations. These challenges ultimately require an improved understanding of the charging limitations of EV battery systems, including the battery electrical behaviour and thermal management, throughout the entire vehicle life.

The battery electrical impedance is related to the voltage-to-current response and heat generation [3], [4]. A theoretical Lithium battery impedance curve is shown in Fig. 1(a) in the Nyquist plot format [5]. The Solid-Electrolyte Interface (R_{SEI}, $X_{C,SEI}$) builds up over time and across cycles at the boundary between the electrode layers and liquid electrolyte [3]. The Charge Transfer impedance (R_{CT}, $X_{C,CT}$) is related to ion intercalation and de-intercalation. The Warburg impedance ($Z_{Warburg}$) represents the mass transport processes in the active materials of the electrodes due to changes in the electrochemical potential. The battery impedance also contains a real component, R_Ω, that reflects the parasitic resistance of the conductors and conductor-to-electrode junctions, and an inductive component, X_L, that reflects the parasitic inductance, which depends on conductor geometry. These features of the battery impedance have all been applied in the EV BMS to improve battery modeling and state-of-charge/degradation estimation [6], [7].

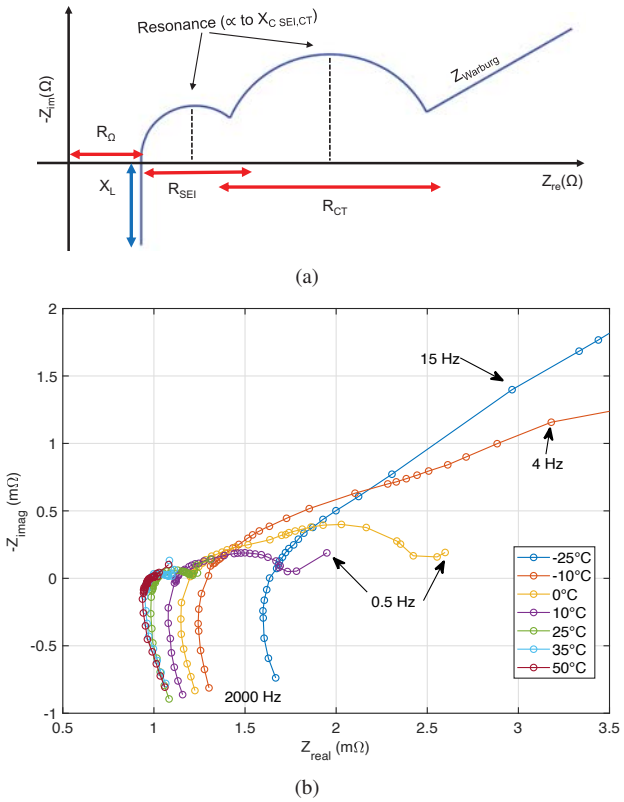

Fig. 1. Lithium battery impedance: (a) idealised impedance curve, and (b) measured 44 Ah NMC pouch cell impedance versus temperature.

The primary factors limiting the time and energy-efficiency of EV fast charging are: 1) the manufacturer-specified maximum voltage limit of the battery cells, 2) the maximum

operating temperature of the battery and conductors, and 3) the heat generated inside each system component. The battery and charging cable electrical impedance are both necessary in the dynamic control of the fast charging current, which dictate the voltage and temperature ramp-up rates. The measured impedance of a 44Ah Lithium Nickel-Manganese-Cobalt-oxide (NMC) pouch battery cell from -25°C to 50°C is shown in Fig. 1(b) [8]. The impedance is measured using Electrochemical Impedance Spectroscopy (EIS), where a perturbation current is injected at fixed frequency, and the voltage response is measured to calculate the impedance phasor [9]. The measured NMC cell impedance increases with reduced temperature, especially at the lowest frequencies, which coincides with the near-dc frequency range of typical constant-current/constant-voltage charging sequences. This phenomenon contributes to the widely-reported degradation of EV range and km-added-per-hour-charging in cold weather conditions [10]. Improving the cold weather battery performance can be achieved through scheduled battery pre-heating, which relies on impedance data. In general, battery pack impedance characterisation throughout the vehicle lifetime is beneficial in maximising the capability of EV and DCFC hardware.

The feasibility of performing Vehicle-level battery EIS (V-EIS) with a DCFC is explored in this study using the systems shown in Fig. 2. A custom DCFC, as shown in Fig. 2(a), is implemented with the CHAdeMO charging standard to interface with the prototype EV and 2015 Nissan Leaf shown in Fig. 2(b). The prototype EV is equipped with the custom liquid-cooled battery pack of Fig. 2(c). To the authors' knowledge, this is the first work to present and analyse measured impedance data from an EV dc charging port. Existing methods for performing EIS inside an EV include cell-level perturbation using the balancing system [8], [11], [12], and pack-level perturbation using one of the vehicle-internal high-voltage power conversion units [11], [13]. Compared to the existing methods, V-EIS enables battery system characterisation without requiring hardware modification inside the EV. Diagnostic information about the charging cable/plug/receptacle may also be obtained. In [14], EIS was used for machine failure diagnosis in wind turbines, and a similar approach to component diagnostics may be taken with EV systems. Finally, since DCFCs are already network-connected, cloud-based impedance data aggregation is feasible with a low incremental DCFC cost that is shared across many users, and no incremental vehicle cost.

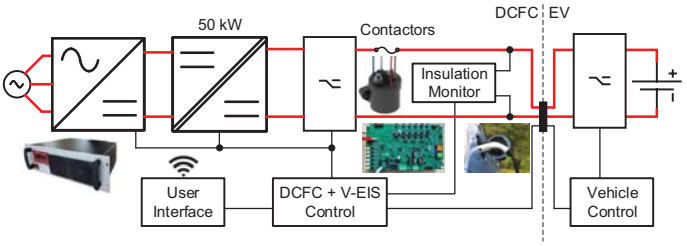

(a)

(b)

(c)

Fig. 2. The systems under study in this work: (a) electrical architecture of a dc fast charge station, (b) prototype EV (left) and Nissan Leaf (right), and (c) custom liquid-cooled 84S2P 88Ah Lithium-NMC battery pack.

II. Charging Port Impedance Model

The primary challenge in utilising the V-EIS impedance data lies in separating the individual impedance of each component perturbed during the test. These components include the charging cable/plug/receptacle, the battery pack, high-voltage wiring, and any of the power conversion units also connected to the charging port during the charging sequence, as shown in Fig. 3. The connected components may be operating during the EIS perturbation sequence, and have variable closed-loop input impedance, e.g. dependent on the input current or output voltage.

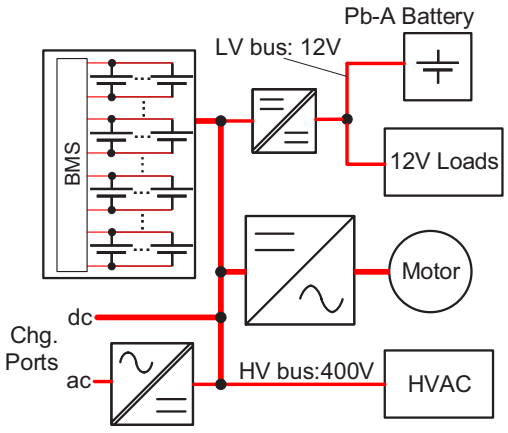

Fig. 3. Simplified EV electrical architecture.

The impedance network used in this study to model

the DCFC-side vehicle input impedance, Z_{in}, is shown in Fig. 4(a). The impedance is referred to the internal DCFC connection to the charging cable, since existing charging standards do not yet implement Kelvin sensing connections within the cable. The charging cable, typically designed to support over 200 A of charging current, introduces the impedance Z_{cable}, consisting of an equivalent series inductance and resistance. The connection interface between the cable and EV introduces a resistance, denoted Z_{plug}. Inside the EV, the dc charging interface is typically routed into a High-Voltage (HV) distribution module, where contactors manage the connection of various HV sources and loads, as shown in Fig. 3. The contactor and HV routing equivalent resistances are shown in Fig. 4(a) as $Z_{contactor}$ and $Z_{routing}$, respectively. Finally, the core EV components modelled in the impedance network are the dc-dc converter, the high-voltage HVAC components (compressor and heater), and the battery pack. The routing impedance, $Z_{routing}$, is variable for each HV module based on its physical location.

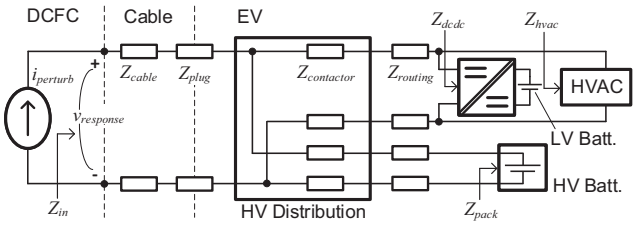

(a)

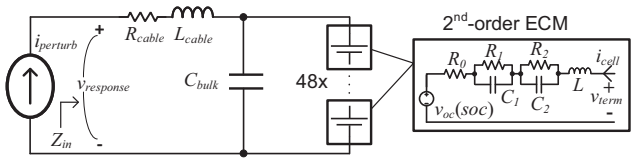

(b)

Fig. 4. (a) dc charging port impedance network. (b) Simplified bulk equivalent model, neglecting contactor and routing impedances.

The model of Fig. 4(a) is simplified to a bulk Z_{in} model, as shown in Fig. 4(b). The simplified model combines Z_{cable} with Z_{plug} as a bulk resistance and inductance. The $Z_{contactor}$ and $Z_{routing}$ are neglected due to their relatively low magnitude. The battery pack impedance, Z_{pack}, is approximated with series-connected 2nd-order Equivalent Circuit Model (ECM) parameters representing series-connected battery groups inside the pack.

III. DC Fast Charger with EIS

The custom DCFC architecture used in this work is shown in Fig. 5. A set of contactors are controlled to transition between fast-charge and V-EIS modes. In fast-charge mode, the DCFC operates according to the CHAdeMO protocol, the ac-dc output voltage, V_{chg}, and the charging receptacle voltage, V_{EV}, are equal. In this state, I_{chg} is the vehicle-requested charging current. In V-EIS mode, the DCFC communicates a low maximum I_{chg} to the EV, and sets V_{chg} to be higher than V_{EV}, such that the linear current source operates with the MOSFET devices in saturation. The digital compensator then regulates the V_{gs} of each current-source phase to track the reference, I_{ref}. The CHAdeMO fast charging protocol allows up to 8 A deviation from the target fast charging current, which is a sufficiently high perturbation amplitude to generate a detectable change in V_{EV} (typically up to 1V). The detailed analysis of the digitally-compensated current source is outside the scope of this work.

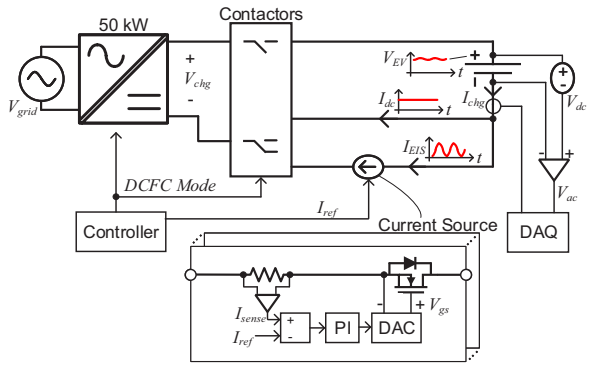

Fig. 5. Fast charger, vehicle EIS current source, and pack voltage response measurement architectures.

In order to ensure the coverage of battery electrochemical effects and explore the effect of vehicle-level component impedances, the target V-EIS frequency is in the range of 0.05 mHz to 3100 kHz. Typical DCFCs have a switching frequency around 8 kHz [15], and do not support the regulation bandwidth required for the target EIS perturbation frequency range. The current source of Fig. 5 only supports uni-directional V-EIS perturbation, which introduces a non-linearity in the battery pack voltage response due to a state-of-charge increase, resulting in an open-circuit voltage increase. This can be compensated by approximating the voltage rise during each perturbation as a linear increase, and applying the offset as a post-processing step. The vehicle response voltage during V-EIS, V_{ac}, is measured by first applying a dc offset, V_{dc}, to V_{EV}, such that the full Data-Acquisition (DAQ) unit input sensing range and resolution can be utilised. Samples of V_{EV} must be obtained between perturbation sequences in order to update V_{dc} with a value that tracks the increasing battery pack open-circuit voltage.

IV. Experimental Results

The custom DCFC implemented in this study is shown in Fig. 6. The digitally-compensated current source is implemented as a single MOSFET phase with a maximum power dissipation of 30 W. The compensator is implemented in a

MAX10M16 FPGA and the high-level DCFC controller is implemented on a SPC560P40L3 micro-controller unit and a PC. All internal system communications occur over one Controller Area Network (CAN), and the DCFC-to-EV communications occur over a separate CAN.

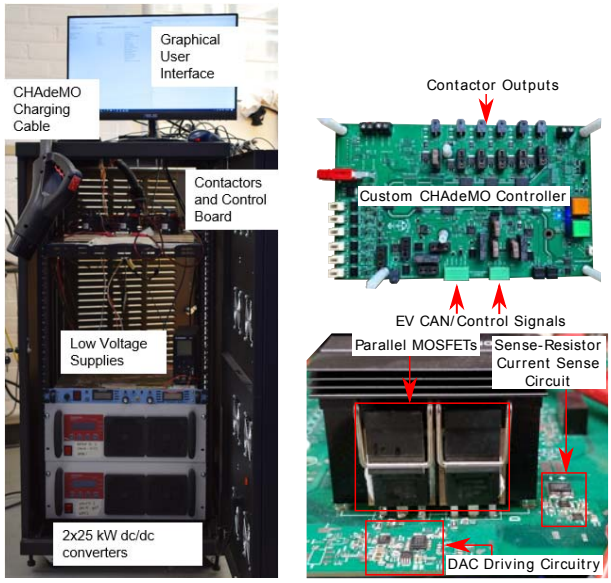

(a) (b)

Fig. 6. (a) The custom DCFC setup (ac-dc stage and voltage response DAQ not shown). (b) The custom CHAdeMO interface control module (top), and the current source module (bottom), with a single phase populated for the V-EIS tests.

The custom DCFC operating in V-EIS mode with a 2015 Nissan Leaf EV (56,000km driven) is shown in Fig. 7. After an initial start-up phase where the 50 kW ac-dc converter ramps its EV-side voltage to 100V, the vehicle connects the battery pack to the charging receptacle, and the DCFC further ramps V_{chg} to V_{EV}+15. The 15V difference between V_{chg} and V_{EV} is necessary to bias the current source MOSFET in saturation, while constraining the thermal loss during V-EIS. After the start-up sequence, the DCFC controller begins to output sinusoidal I_{ref} in order to cycle through the pre-programmed V-EIS perturbation frequencies, and sinusoidal I_{chg} is observed. The DCFC-side voltage response, V_{ac}, is simultaneously measured by the DAQ. A small V_{ac} increase occurs throughout the V-EIS test due to the Nissan Leaf battery pack being charged by the positive I_{chg}, which necessitates re-calibration of V_{dc} throughout the test (not shown).

A. Prototype EV Impedance

In order to demonstrate the detectability of battery-specific impedance changes through measurements of Z_{in}, V-EIS was conducted with the custom DCFC connected to the prototype EV of Fig. 2(b) in two different vehicle configuration modes, with the battery pack at 50% State-of-Charge (SOC). In Vehicle mode, the prototype EV was operated according to Fig. 4(a), with the dc-dc active and HVAC components inactive. In Pack mode, the prototype EV was operated according

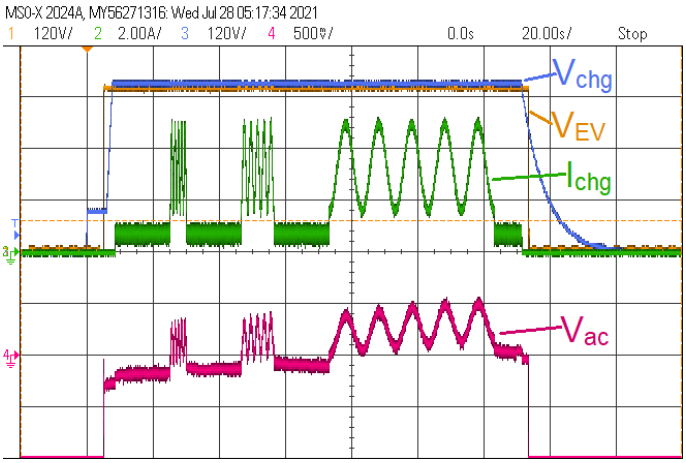

Fig. 7. Fast charger operating in V-EIS mode on the 2015 Nissan Leaf of Fig. 2(b).

to Fig. 8. Removing the active HV components from the prototype EV in Pack mode enables an undistorted measurement of the battery impedance. The V-EIS measurements were also taken with battery temperature, T_{bat}, regulated to 10°C and 25°C using an external liquid chiller unit connected to the battery pack.

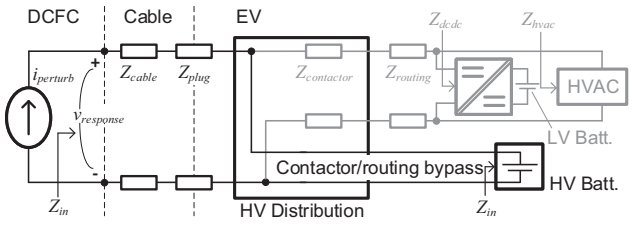

Fig. 8. Pack mode V-EIS configuration in the prototype EV tests. The dcdc and HVAC components are disconnected and the battery pack contactor and routing are bypassed to eliminate their impact on the Z_{in}.

A Pack-versus-Vehicle mode comparison of Z_{in} is shown in Fig. 9. It can be seen that at both temperature points, only the real component of Z_{in} changes at low frequencies, while both the real and imaginary components of Z_{in} change at high frequencies. The real-impedance discrepancy between Pack and Vehicle modes can be attributed to the contactor and HV routing bypass, as shown in Fig. 8. The imaginary-impedance discrepancy at high frequencies in the two modes can be attributed to the presence of parasitic HV cable and routing inductance, and the dc-dc and HVAC components. The dc-dc and HVAC impedance values are likely dominated by their input filter capacitance.

A comparison of Z_{in} under the two coolant temperature set-points is shown in Fig. 10. It can be seen that negligible Z_{in} deviation occurs at high frequencies. At low frequencies, the Z_{in} discrepancy is the same between Vehicle and Pack modes, which indicates that temperature-related changes in pack impedance manifest in the same way regardless of how

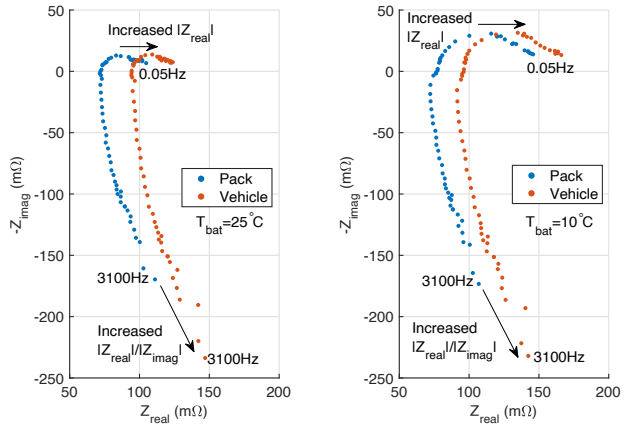

Fig. 9. Prototype EV Z_{in} measurements under pack versus vehicle connection modes.

the DCFC is connected to the vehicle. The battery-related change in Z_{in} shown in Fig. 10 occur at a different frequency range than the component-related change in Z_{in} shown in Fig. 9. This result confirms that battery system diagnostics through the DCFC is possible on the prototype EV.

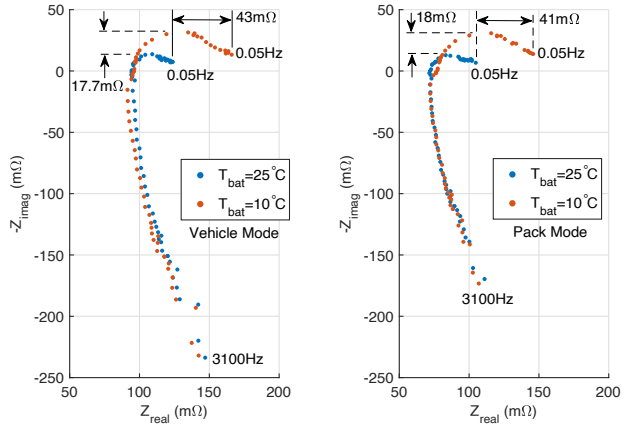

Fig. 10. Prototype EV Z_{in} measurements at 10°C versus 25°C.

B. Nissan Leaf EIS

The measured and modelled Z_{in} of the 2015 Nissan Leaf of Fig. 2(b) are shown in Fig. 11. Compared to the prototype EV impedance curves, the Leaf impedance has a different curvature at frequencies above 100 Hz. This discrepancy may be a result of differences in: HV component count/design, the presence of a dc charge port EMI filter in the Leaf, or parasitic HV routing impedance. A full vehicle teardown, which is outside the scope of this work, would be required to quantify the internal vehicle impedance network for frequencies beyond 100 Hz. In the measured Z_{in} of Fig. 11, it is hypothesized that the bulk equivalent capacitance in parallel with the battery pack, attributable to Z_{dcdc} and Z_{hvac} of Fig. 4(a), enables current to bypass the battery from 100 Hz and higher, leading to a reduction in both the real and imaginary components beyond 1100 Hz (note the y-axis shows -Z_{imag}). At 1850 kHz and beyond, the cable inductance, Z_{cable}, causes the imaginary component to increase. The bulk model parameters shown in Fig. 4(b) were fitted to obtain a reasonable match with the measured data. The measured Leaf impedance increases with a temperature decrease below 100 Hz, which is consistent with the pattern seen in Figs. 10 and 1(b). This result confirms that battery system diagnostics through the DCFC is also feasible on the Nissan Leaf, and likely for other production EVs as well.

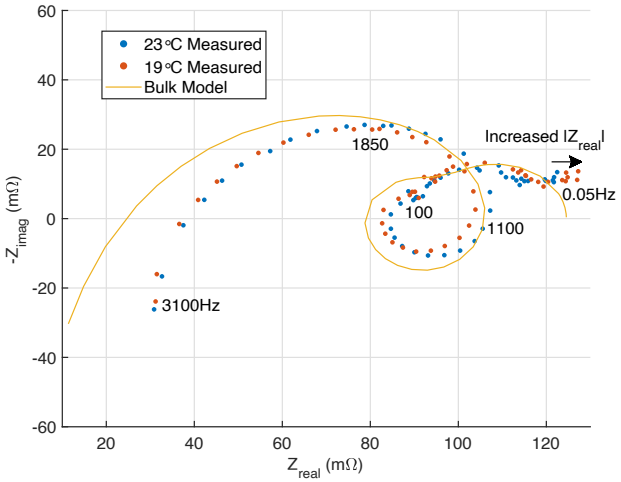

Fig. 11. Simulated and measured Nissan Leaf impedances at 51% SOC.

TABLE I
BULK EQUIVALENT Z_{in} MODEL PARAMETERS

Parameter	Value	Unit
Cell ECM R_0, R_1, R_2	[0.6, 0.39, 0.58]	mΩ
Cell ECM C_1, C_2	[8.96, 70.8]	F
Cell ECM L	0.15	μH
R_{cable}	7.7	$\mu\Omega$
L_{cable}	4	μH
C_{bulk}	1	mF

V. CONCLUSIONS

A custom DCFC with Vehicle-level Electrochemical Impedance Spectroscopy (V-EIS) has been demonstrated. The vehicle input impedance of a custom prototype EV and a Nissan Leaf EV, as seen by the DCFC, was measured across different vehicle high-voltage system connection modes and battery temperatures. In the custom EV, the measured impedance curves exhibit the same temperature-related change when comparing a battery-only connection scheme versus a full-vehicle connection scheme. In the Leaf EV, the measured impedance curves exhibit increasing impedance with

decreasing temperature at frequencies below 100 Hz. These results indicate that battery characterisation and component diagnostics are feasible through V-EIS with the DCFC. This work motivates the future development of charger-side battery diagnostics, including 1) large-scale vehicle fleet battery health monitoring, 2) data collection for improved battery degradation modeling, and 3) direct information exchange with EVs for performance optimisation.

ACKNOWLEDGEMENTS

This work was financially supported by the National Research Council Canada (NRC) Advanced Clean Energy (ACE) Program, Natural Resources Canada (NRCan) through the Office of Energy Research and Development (OERD), and the Natural Sciences and Engineering Research Council of Canada (NSERC).

REFERENCES

[1] "Global ev outlook 2021," 2021. [Online]. Available: https://www.iea.org/reports/global-ev-outlook-2021

[2] "Electric vehicle charging station locations," 2021. [Online]. Available: https://afdc.energy.gov/fuels/electricity_locations.html#/find/nearest?fuel=ELEC

[3] D. Galatro, M. Al-Zareer, C. Da Silva, D. Romero, and C. Amon, "Thermal behavior of lithium-ion batteries: Aging, heat generation, thermal management and failure," *Frontiers in Heat and Mass Transfer*, vol. 14, 05 2020.

[4] A. Moshirvaziri, J. Liu, Y. Arumugam, and O. Trescases, "Modelling of temperature dependent impedance in lithium ion polymer batteries and impact analysis on electric vehicles," in *IECON 2014 - 40th Annual Conference of the IEEE Industrial Electronics Society*, Oct 2014, pp. 3149–3155.

[5] S. Nejad, D. T. Gladwin, and D. A. Stone, "Sensitivity of lumped parameter battery models to constituent parallel-rc element parameterisation error," in *IECON 2014 - 40th Annual Conference of the IEEE Industrial Electronics Society*, 2014, pp. 5660–5665.

[6] H. Rathmann, C. Weber, W. Benecke, J. Eichholz, and D. Kaehler, "Novel methode of state-of-charge estimation using in-situ impedance measurement: Single cells in-situ impedance measurement based state-of-charge estimation for lifepo4 li2to3 battery cells with a real bms," in *IECON 2014 - 40th Annual Conference of the IEEE Industrial Electronics Society*, 2014, pp. 2192–2198.

[7] W. Waag, C. Fleischer, and D. U. Sauer, "Critical review of the methods for monitoring of lithium-ion batteries in electric and hybrid vehicles," *Journal of Power Sources*, vol. 258, pp. 321 – 339, 2014.

[8] Z. Gong, Z. Liu, Y. Wang, K. Gupta, C. da Silva, T. Liu, Z. H. Zheng, W. P. Zhang, J. P. M. van Lammeren, H. J. Bergveld, C. H. Amon, and O. Trescases, "Ic for online eis in automotive batteries and hybrid architecture for high-current perturbation in low-impedance cells," in *2018 IEEE Applied Power Electronics Conference and Exposition (APEC)*, March 2018, pp. 1922–1929.

[9] S. Buller, M. Thele, R. W. A. A. De Doncker, and E. Karden, "Impedance-based simulation models of supercapacitors and li-ion batteries for power electronic applications," *IEEE Transactions on Industry Applications*, vol. 41, no. 3, pp. 742–747, May 2005.

[10] Y. Motoaki, W. Yi, and S. Salisbury, "Empirical analysis of electric vehicle fast charging under cold temperatures," *Energy Policy*, vol. 122, no. C, 7 2018.

[11] A. Kersten, M. Kuder, W. Han, T. Thiringer, A. Lesnicar, T. Weyh, and R. Eckerle, "Online and on-board battery impedance estimation of battery cells, modules or packs in a reconfigurable battery system or multilevel inverter," in *IECON 2020 The 46th Annual Conference of the IEEE Industrial Electronics Society*, 2020, pp. 1884–1891.

[12] E. Din, C. Schaef, K. Moffat, and J. T. Stauth, "A scalable active battery management system with embedded real-time electrochemical impedance spectroscopy," *IEEE Transactions on Power Electronics*, vol. 32, no. 7, pp. 5688–5698, July 2017.

[13] Y. D. Lee, S. Y. Park, and S. B. Han, "Online embedded impedance measurement using high-power battery charger," *IEEE Transactions on Industry Applications*, vol. 51, no. 1, pp. 498–508, Jan 2015.

[14] M. Becherif, A. Henni, M. Benbouzid, and M. Wack, "Impedance spectroscopy failure diagnosis of a dfig-based wind turbine," in *IECON 2012 - 38th Annual Conference on IEEE Industrial Electronics Society*, 2012, pp. 4310–4315.

[15] D. Aggeler, F. Canales, H. Zelaya-De La Parra, A. Coccia, N. Butcher, and O. Apeldoorn, "Ultra-fast dc-charge infrastructures for ev-mobility and future smart grids," in *2010 IEEE PES Innovative Smart Grid Technologies Conference Europe (ISGT Europe)*, 2010, pp. 1–8.